Bulletin of the Seismological Society of America, Vol. 104, No. 1, pp. 439–450, February 2014, doi: 10.1785/0120130059

Validating Nevada ShakeZoning Predictions of Las Vegas Basin Response against 1992 Little Skull Mountain Earthquake Records

by Brady A. Flinchum,* John N. Louie, Kenneth D. Smith, William H. Savran, Satish K. Pullammanappallil, and Aasha Pancha

Abstract Over the last two years, the Nevada Seismological Laboratory has developed and refined Nevada ShakeZoning (NSZ) procedures to characterize earthquake hazards in the Intermountain West. Simulating the M_L 5.6–5.8 Little Skull Mountain (LSM) earthquake validates the results of the NSZ process and the ground shaking it predicts for Las Vegas Valley (LVV). The NSZ process employs a physics-based finite-difference code from Lawrence Livermore Laboratory to compute wave propagation through complex 3D earth models. Computing limitations restrict the results to low frequencies of shaking. For this LSM regional model the limitation is to frequencies of 0.12 Hz, and below. The Clark County Parcel Map, completed in 2011, is a critical and unique geotechnical data set included in NSZ predictions for LVV. Replacing default geotechnical velocities with the Parcel Map velocities in a sensitivity test produced peak ground velocity amplifications of 5%–11% in places, even at low frequencies of 0.1 Hz. A detailed model of LVV basin-floor depth and regional basin-thickness models derived from gravity surveys by the U.S. Geological Survey are also important components of NSZ velocity-model building. In the NSZ-predicted seismograms at 0.1 Hz, Rayleigh-wave minus P-wave ($R - P$) differential arrival times and the pulse shapes of Rayleigh waves correlate well with the low-pass filtered LSM recordings. Importantly, peak ground velocities predicted by NSZ matched what was recorded, to be closer than a factor of two. Observed seismograms within LVV show longer durations of shaking than the synthetics, appearing as horizontally reverberating, 0.2 Hz longitudinal waves beyond 60 s after Rayleigh-wave arrival. Within the basins, the current velocity models are laterally homogeneous below 300 m depth, leading the 0.1 Hz NSZ synthetics to show insufficient shaking durations of only 30–40 s.

Introduction

Over the last three years a group of students at the Nevada Seismological Laboratory (NSL) have been modeling earthquakes on faults surrounding Las Vegas Valley (LVV), using the physics- and geology-based Nevada ShakeZoning (NSZ) process presented by Louie (2008) and Louie, Savran, *et al.* (2011). Savran *et al.* (2011) compared the shaking predicted by NSZ against the statistical U.S. Geological Survey (USGS) ShakeMap results (Wald *et al.*, 1999) and showed dramatic differences in ground amplification. NSZ is a new tool for seismic-hazard analysis to give Nevada engineers and city planners a more realistic and reliable prediction than statistical approaches. With the availability of newly efficient methods of assessing shear velocities within 30 m of the surface (e.g., Louie, 2001), it is now possible to measure accurate and detailed Parcel Maps of geotechnical velocity throughout an entire urban area (Louie, Pullammanappallil, *et al.*, 2011). Based on this cost-effective geotechnical data-collection process, and existing geological and geophysical data on the deeper portions of urban basins, NSZ proves to be an effective predictor of ground motions and amplifications. This paper attempts to validate the NSZ processes, and show that the way basin geometry and geotechnical models are stitched together around Las Vegas will produce synthetic seismograms that match the recorded data.

Simulating the 1992 Little Skull Mountain (LSM) earthquake will confirm that the NSZ process is accurately predicting ground motion and amplification, at least at low frequencies. The LSM earthquake event, at M_L 5.6–5.8, is

*Now at the University of Wyoming, Department of Geology and Geophysics, Dept. 3006, 1000 E. University Avenue, Laramie, Wyoming 82071-2000.

the largest earthquake recorded to occur in Southern Nevada. In addition, ground-motion recordings of this earthquake are available from within LVV. The LVV is the main area of interest for shaking and hazard prediction due to its population, approaching two million; the availability of detailed basin-sediment thickness models (Langenheim *et al.*, 1998, 2001); and detailed geotechnical velocities from the Clark County Parcel Map (Louie, Pullammanappallil, *et al.*, 2011). Clark County, Nevada's Earthquake Parcel Mapping program was a systematic campaign of geotechnical shear-velocity measurements throughout urbanized southern Nevada, completed in 2011 and presented by Louie, Pullammanappallil, *et al.* (2011). Used by Clark County for building-code enforcement, the Parcel Map provides over 10,000 geotechnical shear-velocity measurements to 30 m depth.

This study aims to confirm that the NSZ process can provide accurate predictions of shaking and amplification, with a particular emphasis on the basin response of LVV. Accurate modeling of basin response will confirm Parcel Mapping and Nevada ShakeZoning as effective tools that can help accurately predict earthquake ground motion, hazard, and risk. Comparing the simulations to the LSM data allows sensitivity analyses of the effects of the geotechnical velocity and basin-depth models. With this confirmation, we intend to advance NSZ and simulate ground shaking at higher frequencies.

Methods

Nevada ShakeZoning

The LVV is subject to earthquake hazards from local faults as well as from large seismic events over 100 km away (Su *et al.*, 1998; Smith *et al.*, 2001; Rodgers *et al.*, 2006). Key parameters in modeling earthquake hazards are the characteristics of the rupture, distance from the epicenter, and the shear-wave velocity in the subsurface. In the past, geologic mapping (e.g., Wills *et al.*, 2000) provided statistical estimates of the time-averaged shear velocity in the upper 30 m (denoted here as V_{S30}). Recently, V_{S30} site measurements have become cost effective to collect in large number (Louie, 2001; Louie, Pullammanappallil, *et al.*, 2011), resulting in a Parcel Map containing an accurate geotechnical model of the upper 30 m.

As described by Louie (2008), Louie, Pullammanappallil, *et al.* (2011), and Louie, Savran, *et al.* (2011), NSZ is based on the E3D finite-difference elastic-wave modeling code that Shawn Larsen of Lawrence Livermore National Laboratories designed and validated (Larsen *et al.*, 2001, Larsen *et al.*, 2006). The contribution of NSZ is the combination of different geophysical models describing the geometry and shear-velocity structure of the LVV and surrounding basins in the 3D velocity, density, and Q grids needed for wave computation by E3D. Every scenario compiled by the NSZ process produces a unique set of grid files, illustrated for the LSM scenario in Figure 1. The NSZ process interpolates all of the available geotechnical data into a set of grid files using a distance-weighted average within a specified search radius. Where geotechnical velocity information is lacking within the grid, NSZ assigns default V_{S30} values of 760 m/s in rock, and 500 m/s in basins where sediments are more than 10 m thick (Fig. 1d). The basin models used to create this simulation are the results of Saltus and Jachens (1995) and of Langenheim *et al.* (1998, 2001). The Saltus and Jachens (1995) data yield a rough approximation of basin depths for the entire modeled region. Langenheim *et al.* (1998, 2001) collected additional gravity, borehole, and seismic-reflection data to provide a much more detailed basin model in and around LVV (grid maps in Fig. 1a,b; section in Fig. 1c). The NSZ process also generates two attenuation grid files centered about the peak-modeled frequency. The empirical relations of Olsen *et al.* (2003) for the Los Angeles Basin, provide estimates of Q values for P waves and S waves from the respective velocities assembled at each grid node.

Within LVV, Clark County's Earthquake Parcel Map (Louie, Pullammanappallil, *et al.*, 2011) overrides the default values to accurately represent geotechnical velocities at the surface of the Las Vegas basin (Fig. 1d). Deeper within the basins, NSZ uses average 1D density versus depth curves proposed by Saltus and Jachens (1995) for the entire Basin and Range to estimate density for each grid point. With the density estimate, NSZ then applies Gardner's rule (Gardner *et al.*, 1974) to estimate V_P, then an assumed V_P over V_S ratio of the square root of three to estimate V_S, called V_{Sb} within the basins. Outside the basins and within the bedrock below geotechnical depths, NSZ starts with a 1D regional P-velocity model used for earthquake location from Smith *et al.* (2001), and then estimates density, V_S, and Q values from the same relations used within the basins. The bedrock V_P model includes a Moho at a constant 35 km depth, with the grid extending to 40 km depth. Thus, velocity, density, and Q values below the 300 m deep surface grid zone, within NSZ basins or bedrock, vary with depth, but are uniform with respect to position (section in Fig. 1c). After estimating the five elastic parameters, NSZ applies a minimum V_P criterion of 0.606 km/s and a minimum V_S criterion of 0.35 km/s to every grid node. Because the water table can be greater than 300 m deep in southern Nevada, it is possible for a 300 m thick surface grid node to have a P-wave velocity below 1.5 km/s. Table 1 gives minimum and maximum elastic parameter values across all assembled grid nodes.

Because the grid spacing for wave-propagation computation will be 10 times the 30 m depth of the V_{S30} geotechnical velocities, NSZ obtains the velocities of the upper grid nodes (V_{S300}) by thickness-proportional slowness averaging of the laterally variable geotechnical velocities (V_{S30}) with the laterally homogeneous deep-basin velocities (V_{Sb}). Thus, $V_{S300} = 300/(30/V_{S30} + 270/V_{Sb})$ for Figure 1e. This procedure follows the vertical time-averaging procedure specified in the International Building Code (Building Seismic Safety Council, 1997). With this averaging, the surface-node shear velocity V_{S300} might only vary from 830 to 1000 m/s (20%, black to white in Fig. 1e), even on the Clark County

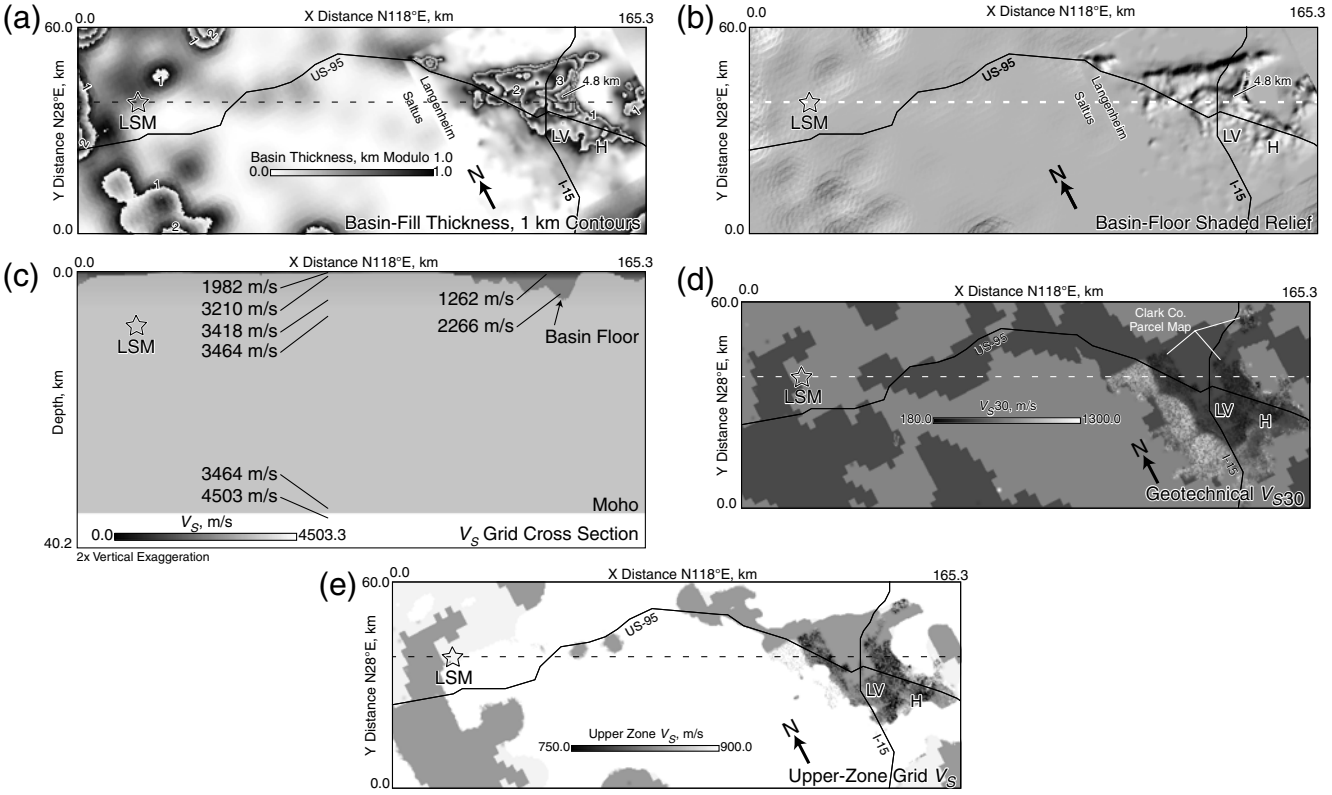

Figure 1. Maps and section illustrating the 300 m resolution computational grid volume assembled by NSZ, showing selected highways, Las Vegas (LV) and Henderson (H) city centers, the 1992 *M* 5.7 Little Skull Mountain (LSM) earthquake epicenter and hypocenter, and the line of section (dashed). (a) Contour map of Neogene volcanic and sedimentary basin-fill thickness. Las Vegas Valley (LVV) details from Langenheim *et al.* (1998, 2001); remainder from Saltus and Jachens (1995). Zero thickness is white, grading to black at 0.99 km thickness, then back to white at 1.0 km thickness, grading to black again at 1.99 km, to white at 2.0 km, etc. Some contours labeled in kilometers. Maximum basin thickness of 4.8 km is flagged. (b) Shaded-relief rendering of basin-floor topography, with sun angle from upper left. (c) Cross section of assembled shear-velocity model, at dashed line on maps. Low velocities are dark; high velocities are lighter in shade. Specific V_S values are called out. (d) Assembled map of V_S averages from the surface to 30 m depth (V_{S30}). Minimum and maximum V_{S30} values on this map are 184 m/s (black) and 1316 m/s (white), respectively. About 9000 Clark County Parcel Map V_{S30} measurements included from Louie, Pullammanappallil, *et al.* (2011). Where not measured, V_{S30} defaults to 760 m/s in bedrock (medium gray) and 500 m/s in basins (dark gray). (e) V_S of assembled upper zone of computational grid, 300 m thick, by slowness averaging. Resulting V_S ranges from 690 to 2731 m/s; any value under 750 m/s renders as black; any value over 900 m/s renders as white.

Parcel Map (Louie, Pullammanappallil, *et al.*, 2011) in which the measured geotechnical V_{S30} varies from 330 to 1000 m/s (200%) over short distances of less than 1 km (black to white in Fig. 1d).

The Little Skull Mountain Earthquake

The LSM Earthquake occurred on 29 June 1992. Its epicenter was roughly 20 km from the proposed Yucca Mountain nuclear waste repository, with latitude of 36.7193° N and longitude of 116.286° W, approximately 120 km northwest of Las Vegas (Fig. 2). Figure 2 shows the moment tensor calculated by the global CMT catalog (described in Dziewonski *et al.*, 1981; Ekström *et al.*, 2012). The LSM event is the largest natural earthquake (not triggered artificially by filling Lake Mead, or by a nuclear explosion) known to occur in southern Nevada and had a local magnitude M_L between 5.6 and 5.8 as estimated by the NSL (Smith *et al.*, 2001). The mainshock of the earthquake was almost completely normal; there was only a small component of left-lateral slip. The hypocenter occurred at a depth of 10–11 km.

The closest recording was 11 km southwest of the mainshock (Fig. 2). Because of the proximity of this station to the event, we used it to calibrate the NSZ source model. This close station experienced an acceleration of 0.206*g* (Smith *et al.*, 2001) with the highest accelerations occurring in the 2–10 Hz band. The Blume and Associates Seismic Safety Program ran the stations that recorded LSM ground motions in LVV. Blume and Associates installed the stations in the 1960s and operated them until the last Nevada nuclear test ended in 1992. The network consisted of three-component analog strong-motion accelerographs (Su *et al.*, 1998; Rodgers *et al.*, 2006). Because the purpose of the recordings was ground-motion validation, they are not referenced to absolute time, only time relative to the trigger time. The NSL had digitized the original analog recordings at 200 samples per second.

Table 1
Ranges of Elastic Parameters Across all 14,766,800 Grid Nodes

Parameter	Minimum	Maximum
V_S, km/s	0.690	4.503
V_P, km/s	1.196	7.800
Density, g/cc	1.820	2.909
Q_S	13.8	2000.0
Q_P	20.7	2000.0

The Little Skull Mountain–Las Vegas Valley Model Area

Nevada ShakeZoning used an angled model area, with an x-axis azimuth of 118° east of north, to produce a rectangular numerical grid of minimum size that included both the LSM epicenter and LVV (Fig. 2). If the modeled area can be smaller, then NSZ can reduce the grid spacing, enabling production of higher frequencies with the same computational effort (Larsen *et al.*, 2001). In order to properly represent a propagating wave at varying velocities, the grid spacing must be small enough to provide at least six grid intervals for the shortest-wavelength wave, of the highest frequency at the lowest velocity.

When selecting the model area for the LSM earthquake, the objective was that NSZ include portions of the basins around the epicenter (Fig. 2). The space allows for basin-wave propagation away from the source and allows the basins between the epicenter and LVV to play an important role in the arrival of seismic energy (Louie, 2008). The model grid used to simulate the LSM earthquake has a uniform spacing of 300 m. According to the lowest default geotechnical velocity V_{S30} of 350 m/s, the simulation allows a maximum frequency of 0.12 Hz without significant grid dispersion artifacts.

A rupture plane oriented to have a strike of N60° E and a dip of 70° SE, following Smith *et al.* (2001) and located according to the main concentration of aftershock hypocenters, simulates the normal fault rupture of the LSM event. Changing the size of a square finite-rupture plane experimentally fine-tuned the seismic moment to match the amplitude on the closest station to the epicenter. After experimentation, a square rupture plane with an area of 16 km^2 was set at a depth 10 km below the surface.

When the plane ruptured into the numerical grid, it ruptured with a −70° rake. Running multiple models with varying hypocenter placement on the fault plane determined that directivity was not an important factor in matching the ST01 records. NSZ and E3D use a Gaussian time-history function for slip velocity at each fault-plane node in the grid (Larsen *et al.*, 2001). This source time function distributes energy evenly for all frequencies up to the specified corner frequency. Rupture propagates at a constant velocity of 2.8 km/s along the fault plane away from the hypocenter. Running the model using a Gaussian source time function with a corner frequency of 0.1 Hz assured limited grid dispersion artifacts. Figure 3 shows synthetic seismograms calculated for the nearest node point to the near-source station ST01 (located on Fig. 2).

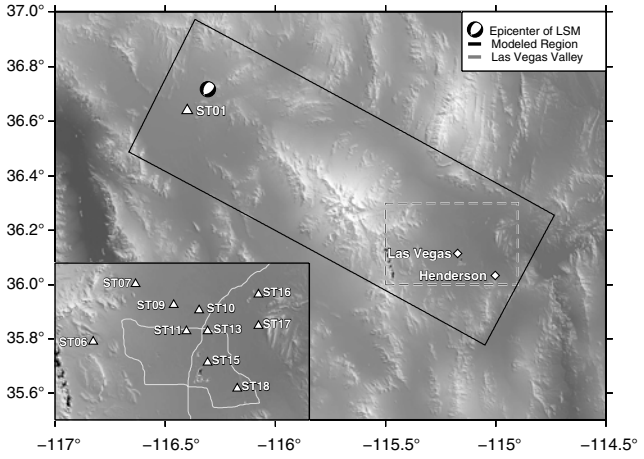

Figure 2. Map setting the numerical grid used to simulate the LSM earthquake (at the focal-mechanism beach ball) into its regional topographic context. Diamonds mark Las Vegas and Henderson, Nevada's two largest cities. The grid x axis is rotated 118° clockwise from north, and the tilted box is the grid area detailed in Figure 1. The inset map of LVV includes principal freeways as well as topography. NSZ computations included no topographic effects. All recording stations shown (triangles) are from the Blume network that recorded the 1992 LSM earthquake. Sedimentary basins of various thicknesses underlie the dark, flat valley areas (Fig. 1a,b).

Data Processing

The NSZ process outputs three-component synthetic velocity seismograms at predetermined locations on the numerical grid, in units of meters per second. A proper comparison of the synthetics to the observed data must first rotate the synthetic seismograms so the positive x axis is facing east. The original orientation of the numerical grid's x axis was 118° clockwise from north. Rotating the synthetic seismograms clockwise by 118° lines up their east–west and north–south components with the observed seismograms, Updating the headers of the observed and synthetic seismogram data files, in Seismic Analysis Code (SAC; Goldstein and Snoke, 2005) format, allows SAC to then rotate all horizontal seismograms to the radial and transverse directions. A final step with SAC converts the recorded accelerograms into velocity seismograms, with a standard trapezoidal integration.

After aligning the recorded and synthetic data and converting the observed seismograms from acceleration into velocity, filtering of both data sets allows more comparisons that are effective. Comparing the spectra of all the observed and synthetic velocity seismograms (e.g., Fig. 3 for the station nearest to the epicenter) showed the existence of a narrow frequency band having both good observed and good synthetic seismograms. Choosing a band-pass filter with

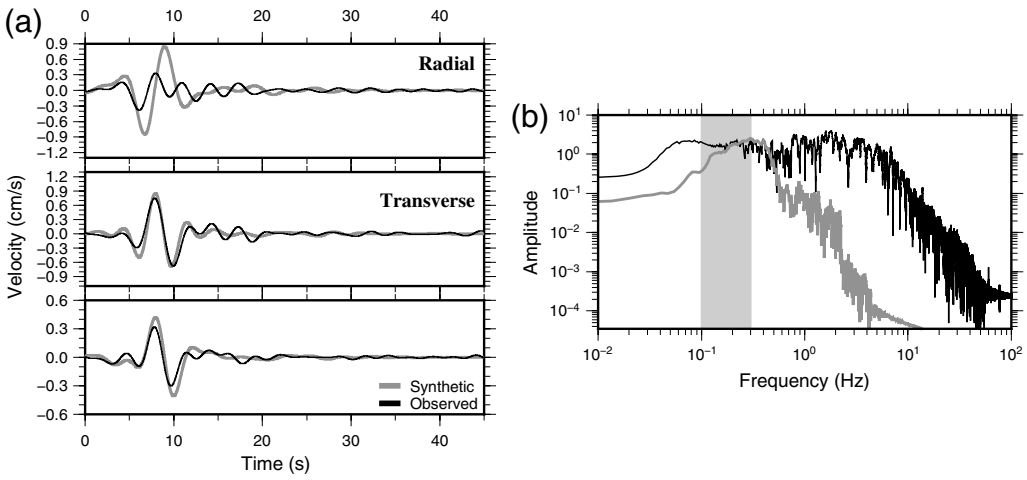

Figure 3. (a) Band-pass-filtered observed, recorded (thin black traces), and ShakeZoning 3D synthetic velocity seismograms (thick gray traces) from the nearest station to the source (ST01, Fig. 2). Observed and synthetic traces are aligned on the first *P*-wave arrival time. The NSZ synthetics are not modeling the extended coda of basin surface waves. (b) Frequency spectra of the NSZ synthetic (gray) and observed (black) seismograms from the LSM scenario. The spectra were computed from the unfiltered transverse component of ST01, shown in (a).

corner frequencies of 0.1 Hz and 0.3 Hz enables comparisons between the observed and recorded seismograms only within this narrow frequency band, in which they both have validity. The Butterworth band-pass filter removed the noisy lower frequencies from the integrated recordings, in which the accelerometers had too little sensitivity (<0.1 Hz); as well as removing the higher frequencies from the synthetics that contain grid dispersion and other numerical artifacts (>0.3 Hz).

Results

An in-depth comparison of differential travel times, horizontal peak ground velocities (PGV), and ground-motion amplifications for the observed and synthetic seismograms followed running the Nevada ShakeZoning simulation for the LSM scenario. Figure 4 compares all of the velocity seismograms computed by the NSZ simulation against the 0.1–0.3 Hz band-passed observed velocity seismograms. Picking *P*-wave arrival times from all the seismograms allowed aligning the synthetics to the observed traces (which lacked absolute time reference) in time for Figure 4. Figure 3 shows Station ST01, 11 km south of the rupture. ST01 is not included in Figure 4, which shows records from LVV. Using ST01 as an initial calibration tool ensured correct estimation of the source parameters for the LSM scenario. It is important that the magnitudes and the first motions matched at this station. Because of the simplistic rupture model and large node spacing, the NSZ source is not perfect.

Figure 4 shows a generally good match between the NSZ synthetics (gray) and the LSM observations (black), over this narrow frequency band. The amplitudes and arrival times of principal phases are close, with waveforms matching quite well at ST06R, ST15T, and ST16T. For many other recordings, the timing and waveforms are very close, but Nevada ShakeZoning has overestimated amplitude, ST07R, ST10R, ST11R, ST15R, and ST17R, though by less than a factor of two. At ST10T, ST13R, and ST17T the phases do not match, but the amplitudes do match. ST13T shows an example of NSZ predicting a major arrival not appearing in the recordings. ST07T, ST10R&T, ST13R, ST15R&T, and ST16R&T are examples of the NSZ synthetics having a shorter duration of shaking than the recordings. The vertical components on the second page of Figure 4 show a similar diversity of matches.

Differential Travel Times

Differential seismic travel times are one tool to analyze the accuracy of the velocity model that the Nevada ShakeZoning process assembles. Instead of analyzing *S* minus *P* ($S-P$) travel times in both the data and synthetics, Rayleigh-wave minus *P*-wave ($R-P$) travel times provided this analysis. The *S* waves have a prominent high-frequency component making them unidentifiable in the synthetics or in the filtered, integrated observed seismograms. It was possible, on the other hand, to pick the *P*-wave times (relative to the start of the record, not absolute) from both the raw recorded accelerograms and the synthetics. The relative Rayleigh-wave times are possible to pick from the filtered records, and from the synthetics at their amplitude peaks.

The overall velocity model for the waves traveling the 120 km between the epicenter and LVV affects the $R-P$ differential travel times the most (Fig. 5). The $R-P$ times picked from the synthetics (diamonds) and the recordings (circles) both produce the upper dashed regression line in Figure 5. This best-fit line represents an average Rayleigh-wave group velocity of $V_r = 2.58$ km/s at 0.1–0.3 Hz. Such a group velocity indicates propagation through mostly bedrock overlain by only shallow (<1 km thick) basins, as shown for the assembled NSZ model in Figure 1a,b. At

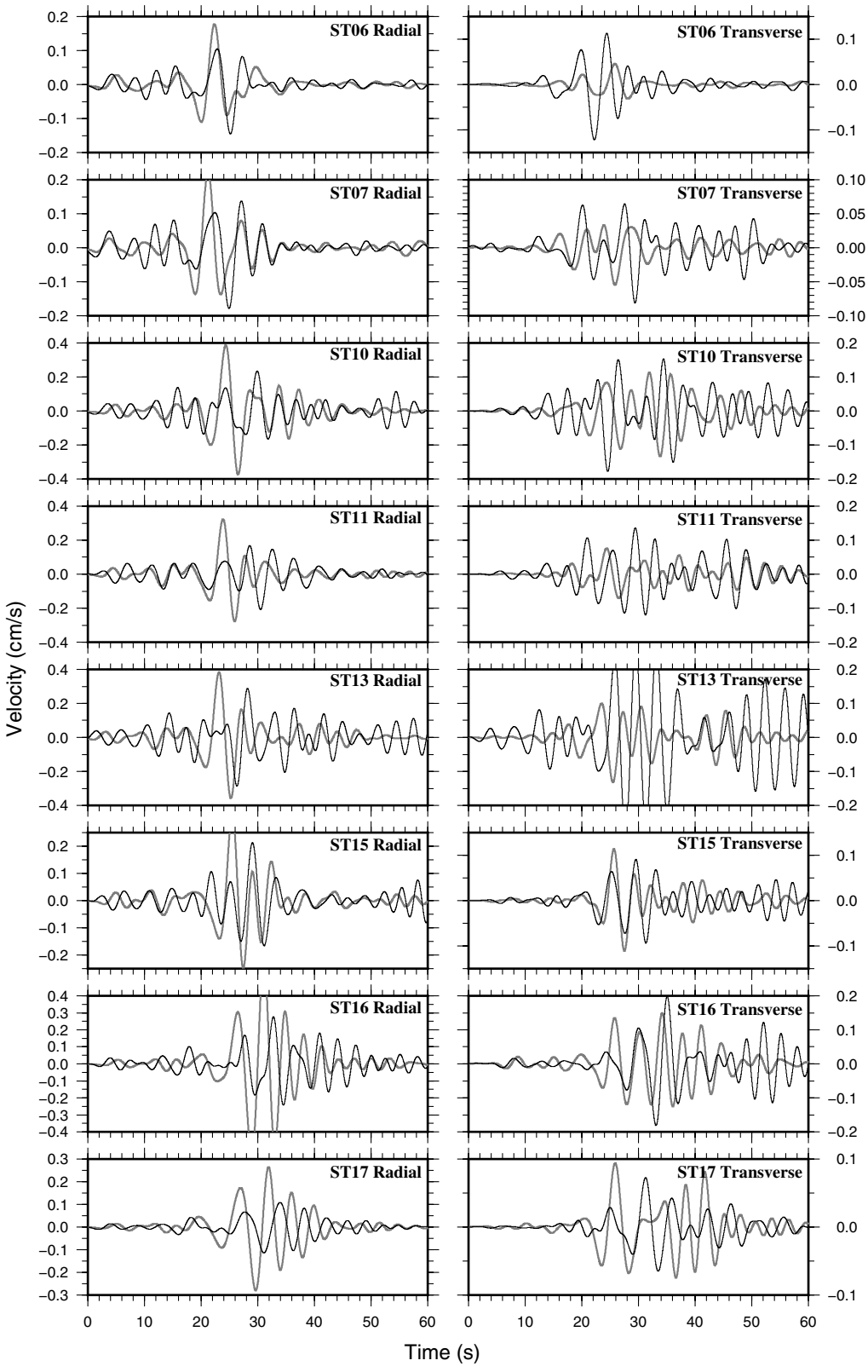

Figure 4. Seismograms from all the stations located by Figure 2 in LVV. Observed (thin black) and synthetic (thick gray) traces are aligned by their *P*-wave first-arrival time picks. A 0.1–0.3 Hz band-pass filter operated on all the seismograms plotted. Vertical axes are ground velocities in units of centimeters per second; horizontal axes are relative time in seconds. (*Continued*)

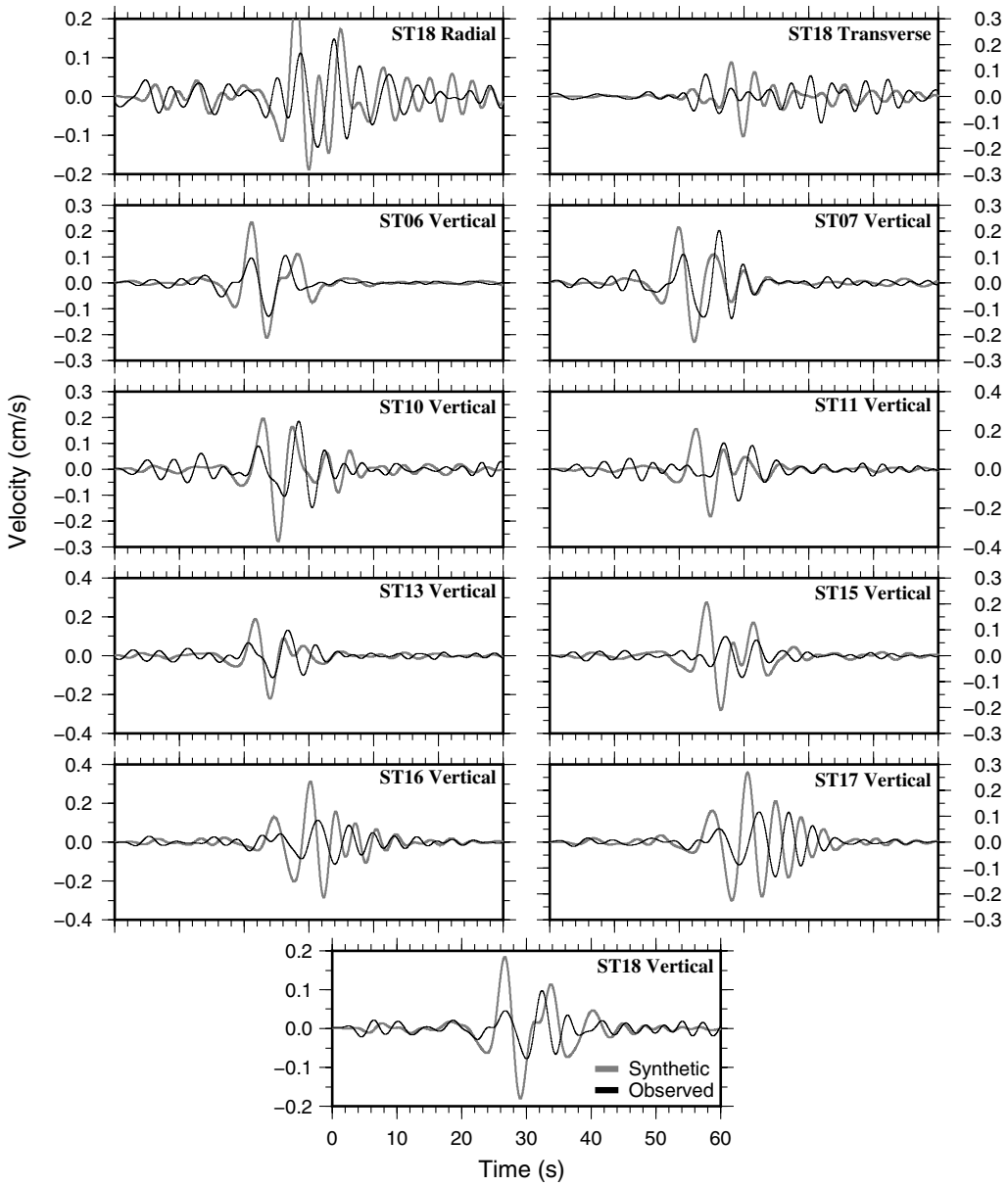

Figure 4. Continued.

0.1–0.3 Hz a 2.58 km/s Rayleigh wave would sense velocity structure from the surface to a quarter-wavelength depth of 3–5 km, with the shallow basins only a minor part of the velocity section.

A prominent limit on the accuracy of NSZ results is the assumption of laterally homogeneous velocities within the basins, below the 30 m thick geotechnical layer and above the basin floor (e.g., the section of Fig. 1c). Although the homogeneous velocities at depth are a broad approximation, the estimates used generally match the $S-P$ and $R-P$ times picked from the observations. The NSZ model uses an upper-crustal P velocity of 6 km/s and an S-wave velocity of V_P divided by the square root of three, or $V_S = 3.46$ km/s. Picking $S-P$ times was possible from the recorded accelerograms (triangles in Fig. 5), regressing to an $S-P$ time versus distance line (lower solid line) implying $V_S = 3.64$ km/s. This velocity observation is only 5% different from the upper-crustal $V_S = 3.46$ km/s NSZ assumes, producing the lower dashed line in Figure 5.

Horizontal Peak Ground Velocities and Amplification

Figure 6 shows the horizontal PGV of shaking produced by Nevada ShakeZoning (white bars) against the PGV data in the integrated and band-pass filtered observed records in two frequency bands. Picking the largest-amplitude velocity from the two horizontal-velocity-filtered seismograms determined the PGV value. PGV changes markedly in the recordings

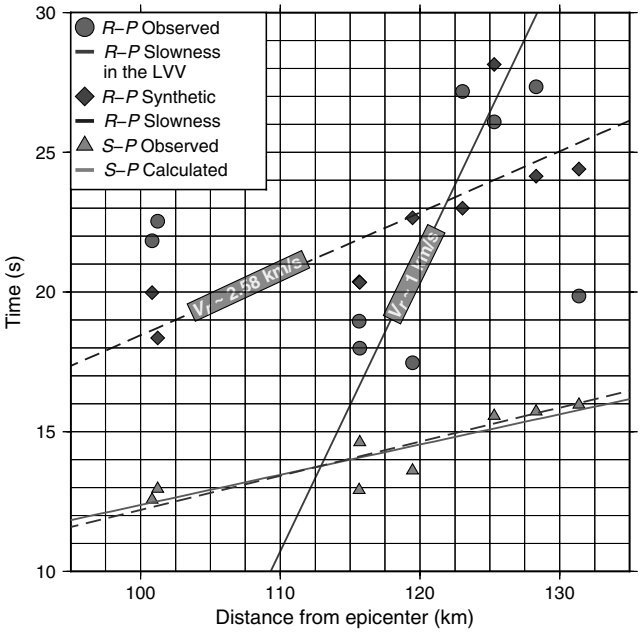

Figure 5. Observed Rayleigh-wave minus *P*-wave ($R - P$) differential travel times (black) for stations in LVV (Fig. 2) according to distance from the epicenter of the LSM earthquake. The $R - P$ times from the synthetics (gray diamonds) are fit by the dashed gray line, computed from $V_r = 2.58$ km/s. Also plotted (dashed and solid lines at the bottom) are calculated $S - P$ times fit from the observed $S - P$ times (triangles) that we picked from the raw accelerograms. The steep black line suggests how an edge-converted Rayleigh wave appears to be traveling at the 1 km/s shear velocity of the upper part of the LV basin.

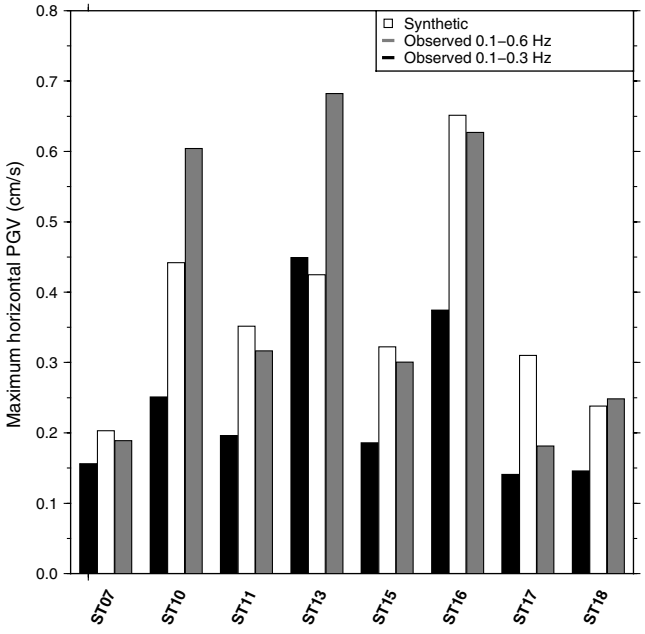

Figure 6. NSZ 0.1 Hz predicted (white bars), and observed horizontal PGV at LLV stations, picked from both band-pass filter ranges for the observed seismograms: 0.1–0.3 Hz (black) and 0.1–0.6 Hz (gray).

between the narrow 0.1–0.3 Hz band that best overlaps the frequency band of the NSZ synthetics, and the broader 0.1–0.6 Hz band that better overlaps the sensitivity band of the Blume accelerometers. The filtered, recorded PGVs at all stations are less than 50% different from the NSZ-predicted PGVs, with the sole exception of station ST17, a rock site on the eastern edge of LVV. In all cases, the recorded PGVs in the narrow 0.1–0.3 Hz band are smaller than the recorded PGVs in the 0.1–0.6 Hz band, due to falling response of the Blume accelerometers below 0.3 Hz. Stations ST10 and ST13 show strong energy between 0.3 and 0.6 Hz, which NSZ cannot predict with this 0.1 Hz computation.

Hazard analysis through examining the amplification of ground motions between rock and soil sites is an important contribution to the work of engineers and city planners. Savran *et al.* (2011) suggested that Nevada ShakeZoning in combination with the Clark County Parcel Map should be more effective than standard USGS ShakeMap methods at predicting amplifications. This study does not include ShakeMap simulation because we cannot compare the ShakeMap results within the narrow frequency band selected here for the ShakeZoning predictions. Frequency greatly influences site-to-site amplifications. The peak amplifications of LVV basin-site records over rock-site records for the LSM earthquake occurred between 0.22 and 0.33 Hz (Rodgers *et al.*, 2006).

The LSM ShakeZoning synthetics have little energy in this frequency band. The areas of amplification should still show up strongly, despite the missing frequencies.

Figure 7 and its accompanying table show observed (black and gray bars) and NSZ-predicted (white bars) PGV amplifications at Blume stations in LVV, in both the 0.1–0.3 Hz (black) and the 0.1–0.6 Hz (gray) frequency bands for the observed. The synthetics (white) overpredict amplifications in the wider 0.1–0.6 Hz band of the recordings (gray), due to the lack of low-frequency energy in the Blume recordings. On the other hand, the synthetics (white) provide a more balanced prediction of the recordings in the narrower 0.1–0.3 Hz band (black). The observations have much more energy in the 0.2–0.3 Hz range, than they have below 0.2 Hz (Su *et al.*, 1998; Rodgers *et al.*, 2006). The amplifications relative to rock-site station ST06 strongly correlate to sedimentary basin thickness, in both narrow and wide frequency bands.

Basin velocity structure and geometry also influence PGV and amplification. Figure 8a shows a standard output from the Nevada ShakeZoning process, the scenario PGV map. Comparing with Figure 1a,b, it is evident that outside the near-source area, the distribution and geometry of sedimentary basins controls where the higher (darker) ground motions will appear. NSZ is taking good advantage of the basin-depth inputs derived from Saltus and Jachens (1995) and Langenheim *et al.* (1998, 2001).

Figure 8b shows the results of a test of the sensitivity of 3D Nevada ShakeZoning PGV predictions to the shallow geotechnical V_{S30} velocities of the Clark County Parcel

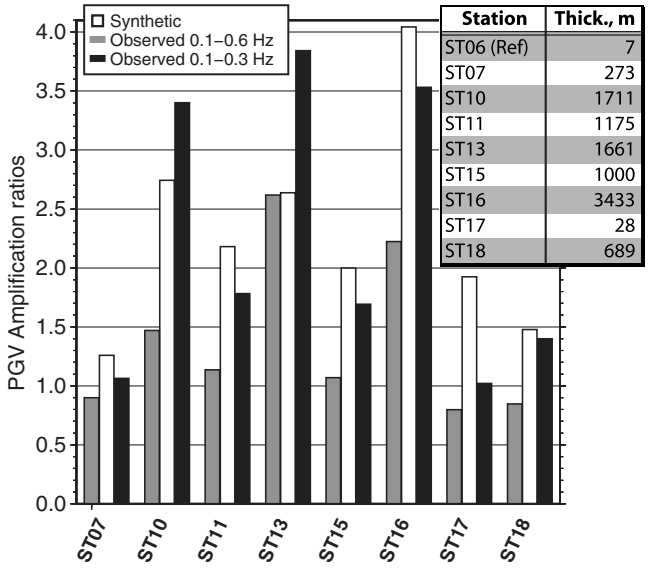

Figure 7. Predicted and observed PGV amplifications at stations in LVV, with respect to rock-site station ST06, in a subbasin at the western edge of LVV (Fig. 1). The white bars show amplifications derived from PGV picked from the NSZ synthetics; gray bars show PGV amplifications picked from the 0.1–0.6 Hz band-pass-filtered observations; and black bars from the 0.1–0.3 Hz filtered observations. ST07 and ST17 are also at the edge of the basin; this is clear because they have less than a 1.4 amplification factor in their observed PGVs. The table shows the basin thickness interpolated from Langenheim *et al.* (1998).

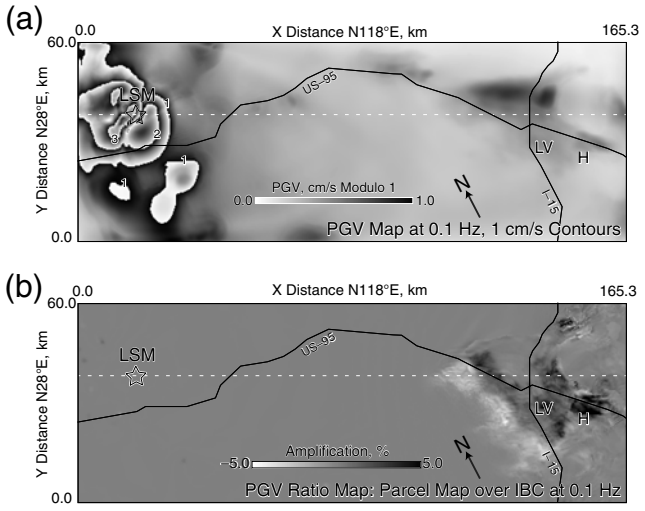

Figure 8. (a) Shaking map of horizontal PGV from E3D computation of the 0.1 Hz LSM scenario across the assembled grid. Zero PGV is white; 0.99 cm/s PGV is black; 1.0 cm/s PGV is white again, etc. PGV contours labeled in cm/s. Minimum computed PGV on this map is 0.028 cm/s; maximum is 3.8 cm/s. (b) PGV ratio map for the sensitivity test of the 0.1 Hz computed scenario shaking ([a] above) to the shallow geotechnical V_{S30} map (Fig. 1d,e above). The maximum amplification of PGV at 0.1 Hz obtained by including the Parcel Map measurements in the model is 10.9% (black above 5%); the minimum is a deamplification of 4.8% (white below 5%). No amplification, a ratio of 1.0, is medium gray.

Map (Louie, Pullammanappallil, *et al.*, 2011; Fig. 1d,e). The map shows PGV ratio across the map, with PGV from the full NSZ model in the numerator, and a model without the geotechnical details in the denominator. The denominator run used only the default 760 m/s rock and 500 m/s soil V_{S30} values in the geotechnical layer, with no site-specific measurements from the Parcel Map or other surveys. There is a great difference in scale between the wavelengths of the NSZ computation at 0.1–0.2 Hz, no shorter than 3750 m; and the 30 m depth extent of the Parcel Map measurements. Despite this difference, Figure 8b shows amplifications of more than 10% (black), as well as deamplifications of almost 5% (white), located in and near areas of low and high geotechnical V_{S30} velocities. The sensitivity test shows the importance of including accurate geotechnical data, even for this low-frequency computation. The test also points out how the wave propagation can spread and channel amplifications away from individual spots of high or low geotechnical velocities.

Discussion and Conclusions

Given the complexity of the LVV basin and the overly simplistic LSM rupture model, the matches between synthetic and recorded seismograms in Figure 4 adequately validate the Nevada ShakeZoning process. It could be said that NSZ often overpredicts shaking, but by less than a factor of two, and we have been conservative here by not using any of the higher-frequency energy in the recordings. At 0.2 Hz and below, the Blume instruments were not very sensitive (Rodgers *et al.*, 2006). In several important ways, ShakeZoning provides shaking predictions with good matches to those recorded from the 1992 LSM earthquake.

Differential Travel Times

Calculating the apparent velocity of observed *S* minus *P* differential travel times versus the distance from the LSM source validates NSZ model properties. Figure 5 shows the agreement between the triangles, and the solid and dashed black lines at the bottom of the graph. Thus, the default *P*-wave and *S*-wave velocities used in the upper crust estimated by NSZ are acceptably representative. Comparing $R - P$ times instead of $S - P$ times was necessary because the Rayleigh waves could be seen on both the synthetic and filtered seismograms, but the *S* body wave arrivals were not visible in the synthetics. Figure 5 shows the linearity of the synthetic Rayleigh-wave minus *P*-wave arrivals (gray diamonds). The synthetic $R - P$ arrivals may be so linear because the strongest of the Rayleigh waves are arriving directly from the LSM source area.

The synthetic $R - P$ picks (gray diamonds fit with dashed gray line in Fig. 5) show one clearly delayed Rayleigh arrival at 125 km distance, at the station that is near the deepest part of the basin. The Rayleigh waves yielding the observed $R - P$ times must be above 0.2 Hz in frequency to make their quarter wavelength smaller than the thickest,

4.8 km part of the basin, resulting in slower Rayleigh propagation and the $R-P$ delay. The synthetic data do not have very much energy above 0.2 Hz, which means that their quarter wavelengths are larger than the basin thickness. These result in faster Rayleigh propagation compared with the higher-frequency observations, because the larger quarter-wavelengths of the synthetics are sensing higher velocities below the basin floor.

Unlike the synthetic data, the observed $R-P$ times (black circles in Fig. 5) do not appear to fit a linear trend with source distance. Around 112 km from the source the observed times show Rayleigh waves arriving earlier than the Rayleigh waves coming from the source area (Fig. 5, circles well below the dashed gray line). Around 120 km distance the Rayleigh waves become delayed and arrive later than the Rayleigh waves coming from the source (Fig. 5, circles well above the dashed gray line). Some of the synthetic $R-P$ times show part of the observed $R-P$ advance or delay. The advanced and delayed Rayleigh waves may well be the result of conversion of earlier P or S waves to Rayleigh waves at an LVV basin edge.

Graves *et al.* (1998) observed and modeled such basin-edge conversions in Santa Monica. The basin edge-converted Rayleigh waves appear to be traveling within the slower basin sediments. Although the filtered velocity seismograms have the majority of their energy at 0.1 Hz, the observations especially have significant energy above 0.2 Hz. The higher-frequency component appears to allow the observations and to some extent the NSZ model to propagate Rayleigh waves through the slower parts of the basin.

Fitting $R-P(x)$ time as a function of source distance to the converted Rayleigh-wave $R-P$ times (Fig. 5, steep solid line); and to the $R-P$ times of the Rayleigh waves traveling from the source (dashed gray line), gives two estimates of Rayleigh-wave velocity. Equation (1) solves for the Rayleigh-wave velocity V_r:

$$R-P(x)=\frac{x}{V_r}-\frac{x}{V_P}, \tag{1}$$

in which x is the distance from the source and $R-P(x)$ is the slope of the line shown in Figure 5. Solving a similar equation with V_r replaced by V_S, using the slope of the $S-P(x)$ line observed from the Blume stations (Fig. 5, solid dark line at bottom) finds the P-wave velocity V_P. Figure 5 shows the calculated velocities of the two Rayleigh-wave phases. The Rayleigh-wave velocity for the synthetics remains high in the LVV basin, because at 0.1 Hz the wavelength is 10–26 km and Rayleigh-propagation velocity is not strongly affected by the relatively shallow basin, with a thickness not exceeding 4.9 km (Langenheim *et al.*, 1998, 2001). The converted Rayleigh waves traveling in the thickest part of the LVV basin are traveling at 1 km/s. This is a reasonable value for Rayleigh waves in the upper kilometer or two of the basin.

Amplification Discussion

The NSZ-predicted basin-over-rock-site PGV amplification factors are within a factor of two of the amplification observed by the Blume network, for all stations. Figure 7 shows the amplifications with respect to rock-site station ST06, for both a narrowband 0.1–0.3 Hz band-pass filter applied to the Blume recordings (black bars), and a broaderband 0.1–0.6 Hz filtering (gray bars). Frequency differences can explain the discrepancies between the synthetic (white bars) and observed amplifications (black and gray bars). Making the quarter-wavelength approximation, the highest amplifications should occur when a quarter of the Rayleigh wavelength matches the basin thickness. Assuming the calculated Rayleigh-wave velocity of 2.6 km/s, the wavelength of a 0.1 Hz surface wave would be 26 km. With a wavelength of 26 km the maximum amplification would occur if the basin were 6.5 km deep. At its deepest, the LVV basin is only 4.8 km deep (Langenheim *et al.*, 1998, 2001), and most of the basin is less than 3 km deep. The Nevada ShakeZoning synthetics should predict the maximum amplification at ST16, the deepest point in the LVV. This assumption holds when looking at Figure 7, as the maximum amplification for the synthetics occurs at ST16. The observed data show the greatest amplifications at ST10 and ST13 (gray bars), but only for the 0.1–0.6 band-pass-filtered band that includes frequencies over 0.3 Hz. Given a Rayleigh-wave velocity of 2.58 km/s the maximum amplification should occur between 0.2 and 0.4 Hz, which is consistent with what past studies have observed (Su *et al.*, 1998; Rodgers *et al.*, 2006). The NSZ-modeled LSM scenario earthquake has a shortage of energy in this higher-frequency range, which results in predicting less PGV amplification than observed.

The geotechnical velocities measured by the Clark County Parcel Map strongly affect ground shaking in LVV, even at low frequencies (Louie, Pullammanappallil, *et al.*, 2011; Louie, Savran, *et al.*, 2011). However, NSZ scenario computations show that the PGV amplification due to a soft spot on the Parcel Map, or the deamplification due to a hard spot, are not contained to just the areas of anomalous geotechnical velocity identified by the Parcel Map. Figure 8b shows the PGV-ratio map for the sensitivity test of the 0.1 Hz NSZ shaking predictions to the V_{S30} values in the Clark County Parcel Map (shown in Fig. 1d,e). Running the complete scenario shaking prediction on two different models, including the Parcel Map, and then using only the NEHRP-default V_{S30} values, allows finding the PGV ratio map. For the 0.1 Hz NSZ prediction, amplifications, and deamplifications average about 5% and do not exceed 11%. It is notable that amplifications spread out in the direction of wave propagation from the scenario earthquake, causing the streaking seen near Henderson on Figure 8b. In the higher frequency, 0.5 Hz scenarios computed by Louie, Pullammanappallil, *et al.* (2011), Louie, Savran, *et al.* (2011), and by Savran *et al.* (2011), amplifications and deamplifications due to the Parcel Map exceed a factor of two.

Louie (2008) also observed an NSZ PGV basin amplification factor in LVV that increases strongly as the basin thickens from 1 to 2 km. Figure 7 shows that predicted and observed amplifications agree closely for stations at basin thicknesses of less than 1.5 km. Between thicknesses of 1.5 and 2.0 km, the observed amplifications exceed a factor of three, whereas the NSZ-predicted amplifications are barely a factor of two. At the station having a basin thickness of 3.6 km—similar to the depth of Rayleigh-wave quarter-wavelength sensitivity at 0.1 Hz—the predicted amplification better matches the observed factor of three.

Peak Ground Velocity Discussion

One of the most important aspects of Nevada ShakeZoning to validate is its ability to predict horizontal ground motion. Peak horizontal ground motion is an important input parameter for the work of engineers, city planners, and emergency responders. The ability of Nevada ShakeZoning to predict ground motions once again is frequency dependent. Higher frequency and shorter wavelength allow the waves to be properly represented within the geometries of the basins. The Clark County Parcel Map (Louie, Pullammanappallil, *et al.*, 2011) and the (Langenheim *et al.*, 1998, 2001) basin thicknesses have the most prominent effects on the distribution of PGVs for the LSM scenario, which occurred outside the basin. Figure 6 shows the horizontal PGV of the synthetics (white bars) and the integrated, band-pass-filtered data in two frequency ranges (black bars for 0.1–0.3 Hz, and gray bars for 0.1–0.6 Hz). The recorded peak ground velocities are within a factor of two of the synthetic peak ground velocities at all stations.

Duration of Shaking

In the comparison between observed and synthetic seismograms at 0.1 Hz in Figure 4, it is clear that an observation that is not modeled well by NSZ is the duration of shaking. The synthetics match the main Rayleigh-wave pulses very well in their peak ground velocity and reasonably well in their timing and phase. But the very strong, very late-arriving surface-wave pulses appearing in the observations above 0.2 Hz from stations ST10, ST13, ST16, and ST17 (Fig. 4) are not modeled. The pulses exceed 10 s duration and can arrive more than 60 s after the main Rayleigh pulse (as seen on the original data) at these stations, which are the deep-basin stations (Fig. 7). The NSZ synthetics do contain extended coda of horizontally reverberating surface waves within the basins, at least to about 30 s. However, the synthetic coda amplitudes are only about half the amplitudes of the observed coda, in and out of the LVV basin.

Louie (2008), Louie, Pullammanappallil, *et al.* (2011), Louie, Savran, *et al.* (2011), and Savran *et al.* (2011) have all observed relatively higher-amplitude coda on synthetics computed at higher frequencies than 0.1 Hz. Their models of earthquake scenarios more proximal to the Las Vegas basin do show much stronger and later-arriving surface waves. (No observations of such proximal earthquakes yet exist for validation.) These coda elements appear to originate in conversions of body-wave energy at basin edges, to surface waves propagating slowly across the basins and reverberating horizontally off geotechnical heterogeneities within the basins, and off other parts of the basin edges. This observation, also made by Rodgers *et al.* (2006), suggests the role that the very low 0.1 Hz frequency of the NSZ synthetics, for the LSM scenario, play in the mismatch to the recordings. At such a low frequency, the modeled basin edges and interior heterogeneity are not reflective enough to trap as much energy within the basins, compared to the higher-frequency (>0.2 Hz) surface waves observed.

With the exception of the extended, late coda waves, the LSM recordings effectively validate our Nevada ShakeZoning synthetics. As a 3D, physics-based community seismic modeling environment, Nevada ShakeZoning has similar goals to the work of Frankel *et al.* (2007) in Seattle. ShakeZoning cannot match waveforms to the accuracy achieved by Olsen (2000), for example, in the Los Angeles Basin. Nevertheless, it provides the Nevada community with a means of anticipating the effects of scenario earthquakes that is much more realistic than 1D estimates, such as ShakeMap (Wald *et al.*, 1999). The presence of multiple sedimentary basins with complex 3D geometry amplifies, directs, and extends ground shaking in ways, which ShakeMap cannot predict (Olsen *et al.*, 2006). Las Vegas is a locality both well characterized, with the completion of Clark County's Parcel Map, and vital to the economy of the state of Nevada. It is incumbent on seismologists to give the community better guidance, even if imperfect.

Data and Resources

Nevada ShakeZoning open-source model-assembly codes, geotechnical and basin data sets, and results including papers, presentations, and scenario wave-propagation animations are available at http://crack.seismo.unr.edu/NSZ/ (last accessed August 2013). The Clark County Parcel Map is available from http://www.clarkcountynv.gov by searching for the OpenWeb Seismic Class Map (last accessed August 2013). The ground-motion data used in this study are archived by the NSL, who have made them available at http://crack.seismo.unr.edu/NSZ/LSM-Blume-data.tar.gz (last accessed August 2013). All digital elevation data that were used to generate maps in this study were obtained from through the U.S. Geological Survey's Earth Resources Observation and Science (EROS) Center and can be accessed at http://earthexplorer.usgs.gov (last accessed February 2013).

Acknowledgments

Optim Inc. and the Nevada Applied Research Initiative funded the CCoG computing cluster. Werner Hellmer P.E. of the Clark County, Nevada, Development Services Department gave permission for us to use the Parcel Map. Optim Seismic Data Solutions and the NSL at the University of Nevada, Reno (UNR), provided seed funding. This research was partially

supported by the Southern California Earthquake Center (SCEC). SCEC is funded by NSF Cooperative Agreement EAR-0106924 and USGS Cooperative Agreement 02HQAG0008. The SCEC contribution number for this paper is 1594. This research was also partly supported by the USGS, Department of the Interior, under USGS Award Numbers 07HQGR0029, 08HQGR0046, G09AP00050, G09AP00051, and G10AP00002. The views and conclusions contained in this document are those of the authors and should not be interpreted as necessarily representing the official policies, either expressed or implied, of the U.S. Government. Richard Saltus, Bob Jachens, and Victoria Langenheim of the USGS kindly made their basin-thickness results available to us. We also thank Barbara Luke of University of Nevada, Las Vegas, for assembling her database of geotechnical shear velocities in Las Vegas.

References

Building Seismic Safety Council (BSSC) (1997). *NEHRP Recommended Provisions for Seismic Regulations for New Buildings and Other Structures, Part 1: Provisions*, Federal Emergency Management Agency, Washington D.C., 302 pp.

Dziewonski, A. M., T. -A. Chou, and J. H. Woodhouse (1981). Determination of earthquake source parameters from waveform data for studies of global and regional seismicity, *J. Geophys. Res.* **86,** 2825–2852

Ekström, G., M. Nettles, and A. M. Dziewonski (2012). The global CMT project 2004–2010: Centroid-moment tensors for 13,017 earthquakes, *Phys. Earth Planet. Int.* **200–201,** 1–9.

Frankel, A. D., W. J. Stephenson, D. L. Carver, R. A. Williams, J. K. Odum, and S. Rhea (2007). Seismic hazard maps for Seattle, Washington, incorporating 3D sedimentary basin effects, nonlinear site response, and rupture directivity, *U.S. Geol. Surv. Open-File Rept. 2007-1175*, 82 pp.

Gardner, G. H. F., L. W. Gardner, and A. R. Gregory (1974). Formation velocity and density—The diagnostic basics for stratigraphic traps, *Geophysics* **39,** 770–780.

Goldstein, P., and A. Snoke (2005). SAC availability for the IRIS community, Incorporated Institutions for Seismology Data Management Center Electronic Newsletter, available at http://www.iris.edu/news/newsletter/vol7no1/page1.htm (last accessed November 2013).

Graves, R. W., A. Pitarka, and P. G. Somerville (1998). Ground motion amplification in the Santa Monica area: Effects of shallow basin edge structure, *Bull. Seismol. Soc. Am.* **88,** 1224–1242.

Langenheim, V. E., J. A. Grow, R. C. Jachens, G. L. Dixon, and J. J. Miller (2001). Geophysical constraints on the location and geometry of the Las Vegas Valley shear zone, Nevada, *Tectonics* **20,** 189–209.

Langenheim, V. E., J. Grow, J. J. Miller, J. D. Davidson, and E. Robison (1998). Thickness of Cenozoic deposits and location and geometry of the Las Vegas Valley shear zone, Nevada, based on gravity, seismic-reflection, and aeromagnetic data, *U.S. Geol. Surv. Open-File Rept. OF98-0576*, available at http://pubs.usgs.gov/of/1998/0576/report.pdf (last accessed November 2013).

Larsen, S., D. Dreger, and D. Dolenc (2006). Simulations of the 1906 San Francisco earthquake using high performance computing, *Seismol. Res. Lett.* **77,** 275.

Larsen, S., R. Wiley, P. Roberts, and L. House (2001). Next-generation numerical modeling: Incorporating elasticity, anisotropy and attenuation, *SEG Expanded Abstr.* **20,** 1218–1221.

Louie, J. N. (2001). Faster, better: Shear-wave velocity to 100 meters depth from refraction microtremor arrays, *Bull. Seismol. Soc. Am.* **91,** 347–364.

Louie, J. N. (2008). Assembling a Nevada 3-D velocity model: Earthquake-wave propagation in the Basin & Range, and seismic shaking predictions for Las Vegas, *SEG Expanded Abstr.* **27,** 2166–2170.

Louie, J. N., S. K. Pullammanappallil, A. Pancha, T. West, and W. K. Hellmer (2011). Earthquake hazard class mapping by parcel in Las Vegas Valley, in *Proc. of the American Society of Civil Engineers (ASCE) 2011 Structures Congress*, 14 April 2011, 1794–1805, doi: 10.1061/41171(401)156.

Louie, J. N., W. Savran, B. Flinchum, G. Plank, G. Kent, K. D. Smith, S. K. Pullammanappallil, A. Pancha, and W. K. Hellmer (2011). Next-Level ShakeZoning for earthquake hazard definition in the Intermountain West, in *Proc. of the 2011 Symposium on Engineering Geology and Geotechnical Engineering (EGGE)*, March 25, Las Vegas, Nevada, 15 pp. (Reprint at http://crack.seismo.unr.edu/ma/scenarios/Louie-11EGGE.pdf; last accessed November 2013.)

Olsen, K. B. (2000). Site amplification in the Los Angeles Basin from three-dimensional modeling of ground motion, *Bull. Seismol. Soc. Am.* **90,** S77–S94.

Olsen, K. B., S. M. Day, and C. R. Bradley (2003). Estimation of *Q* for long-period (> 2 sec) waves in the Los Angeles Basin, *Bull. Seismol. Soc. Am.* **93,** 627–638.

Olsen, K. B., S. M. Day, J. B. Minster, Y. Cui, A. Chourasia, M. Faerman, R. Moore, P. Maechling, and T. Jordan (2006). Strong shaking in Los Angeles expected from asouthern San Andreas earthquake, *Geophys. Res. Lett.* **33,** L07305, doi 10.1029/2005GL025472.

Rodgers, A., H. Tkalcic, D. McCallen, S. Larsen, and C. Snelson (2006). Site response in Las Vegas Valley, Nevada from NTS explosions and earthquake data, *Pure Appl. Geophys.* **163,** 55–80.

Saltus, R. W., and R. C. Jachens (1995). Gravity and basin-depth maps of the Basin and Range Province, Western United States, *U.S. Geol. Surv., Geophysical Investigations Map*, Report: GP-1012, 1 sheet.

Savran, W. H., B. Flinchum, G. Plank, C. Dudley, N. Prina, and J. N. Louie (2011). Comparing physics-based Next-Level ShakeZoning computations with USGS ShakeMap statistics for So. NV earthquake scenarios, in *Proc. of the 2011 Symposium on Engineering Geology and Geotechnical Engineering (EGGE)*, March 25, Las Vegas, Nevada, 15 pp. (Reprint at http://crack.seismo.unr.edu/ma/scenarios/Savran-EGGEPaper_Final.pdf.)

Smith, K. D., J. N. Brune, D. dePolo, M. K. Savage, R. Anooshehpoor, and A. F. Sheehan (2001). The 1992 Little Skull Mountain earthquake sequence, southern Nevada Test Site, *Bull. Seismol. Soc. Am.* **91,** 1595–1606.

Su, F., J. Anderson, S. Ni, and Y. Zeng (1998). Effect of site amplification and basin response on strong motion in Las Vegas, Nevada, *Earthq. Spectra* **14,** 357–376.

Wald, D. J., V. Quitoriano, T. H. Heaton, H. Kanamori, C. W. Scrivner, and C. B. Worden (1999). TriNet "ShakeMaps:" Rapid generation of instrumental ground motion and intensity maps for earthquakes in Southern California, *Earthq. Spectra* **15,** 537–556.

Wills, C. J., M. D. Petersen, W. A. Bryant, M. S. Reichle, G. J. Saucedo, S. S. Tan, G. C. Taylor, and J. A. Treiman (2000). A site-conditions map for California based on geology and shear wave velocity, *Bull. Seismol. Soc. Am.* **90,** S187–S208.

Nevada Seismological Laboratory
University of Nevada, Reno
Reno, Nevada 89557
(B.A.F., J.N.L., K.D.S., W.H.S.)

Optim, Inc.
200 South Virginia St., Suite 560
Reno, Nevada 89501
(S.K.P., A.P.)

Manuscript received 7 March 2013;
Published Online 21 January 2014